

DOI: 10.1002/cssc.201402057

A Tailored Catalyst for the Sustainable Conversion of Glycerol to Acrolein: Mechanistic Aspect of Sequential Dehydration

Danim Yun,^[a] Tae Yong Kim,^[a] Dae Sung Park,^[a] Yang Sik Yun,^[a] Jeong Woo Han,^[b] and Jongheop Yi^{*[a]}

Developing a catalyst to resolve deactivation caused from coke is a primary challenge in the dehydration of glycerol to acrolein. An open-macropore-structured and Brønsted-acidic catalyst (Marigold-like silica functionalized with sulfonic acid groups, MS-FS) was synthesized for the stable and selective production of acrolein from glycerol. A high acrolein yield of 73% was achieved and maintained for 50 h in the presence of the MS-FS catalyst. The hierarchical structure of the catalyst with macropores was found to have an important effect on the stability of the catalyst because coke polymerization and pore blocking caused by coke deposition were inhibited. In addition, the behavior of 3-hydroxypropionaldehyde (3-HPA) during the se-

quential dehydration was studied using density functional theory (DFT) calculations because 3-HPA conversion is one of the main causes for coke formation. We found that the easily reproducible Brønsted acid sites in MS-FS permit the selective and stable production of acrolein. This is because the reactive intermediate (3-HPA) is readily adsorbed on the regenerated acid sites, which is essential for the selective production of acrolein during the sequential dehydration. The regeneration ability of the acid sites is related not only to the selective production of acrolein but also to the retardation of catalyst deactivation by suppressing the formation of coke precursors originating from 3-HPA degradation.

Introduction

Since the demand for a clean and green technology has increased, countless efforts have been made to replace conventional petrochemical processing. Biomass could be a solution to satisfy the needs of the times because it has a potential for producing fine chemicals or building blocks without increasing greenhouse gas emissions.^[1,2] Therefore, various studies concerning the production of value-added chemicals from bio-based compounds have been reported in recent years.^[3–6] In particular, the conversion of glycerol to acrolein has attracted a considerable amount of attention as an alternative route to the production of acrolein from petroleum-based propylene.^[7–9] Furthermore, an increasing cost ratio of acrolein to glycerol in recent years makes the conversion also economical-

ly viable.^[10] Hence, the conversion of glycerol and the related catalysts have been extensively studied.^[8–11]

Thanks to previous studies, a better understanding has been developed regarding the mechanism of glycerol conversion^[10,12,13] and the effectiveness of Brønsted acid catalysts.^[7,14–17] During glycerol conversion, a variety of reactions can take place, but the desired reaction are two sequential dehydrations consisting of the dehydration of glycerol to 3-hydroxypropionaldehyde (3-HPA) and 3-HPA to acrolein. When Brønsted acid catalysts are used, the first dehydration, known as the rate-determining step,^[14,18] can be easily induced. This can be attributed to the secondary OH group of glycerol being preferentially adsorbed onto the Brønsted acid sites, which should occur prior to the dehydration to 3-HPA.^[7,14] Although Brønsted acid catalysts show a high activity and selectivity for acrolein early in the reaction, the catalysts are quickly deactivated due to extensive coke deposition.^[8,19] Therefore, solving the problem of coke formation is necessary to achieve glycerol dehydration on a commercial scale.

There are two approaches to solve the problem of this type of deactivation. One involves reducing the amount of coke produced during the reaction and the other is enhancing intrinsic resistivity to coke deposition. For the former, a key to the solution involves 3-HPA conversion. 3-HPA is considered to be a major intermediate formed during the reaction as it is a precursor of acrolein.^[12,15] It is very reactive, and the additional undesired conversions can easily take place, resulting in coke formation.^[10,12,15] However, the behavior of 3-HPA during glycerol dehydration is not well understood currently because

[a] D. Yun,[†] T. Y. Kim,[†] D. S. Park, Y. S. Yun, Prof. J. Yi
World Class University (WCU) program of
chemical Convergence for Energy & Environment
Institute of Chemical Processes
School of Chemical and Biological Engineering
Seoul National University
Seoul 151-741 (Republic of Korea)
Fax: (+82) 2-885-6670
E-mail: jyj@snu.ac.kr

[b] Prof. J. W. Han
Department of Chemical Engineering
University of Seoul
Seoul 130-743 (Republic of Korea)

[†] These authors contributed equally to the work.

 Supporting Information for this article is available on the WWW under
<http://dx.doi.org/10.1002/cssc.201402057>.

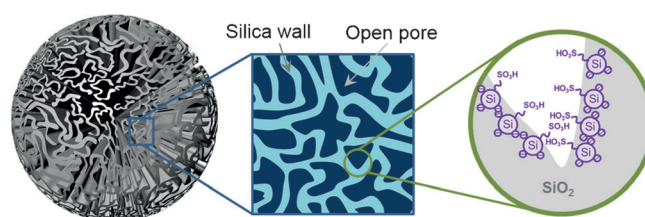
the detection of 3-HPA is almost impossible during the reaction due to the highly reactive nature of 3-HPA. A theoretical study could contribute to a better understanding of this problem, but up to now such studies have been limited to the reaction mechanism of glycerol.^[13,14] It should be possible to observe the behavior of 3-HPA during the reaction using density functional theory (DFT) calculations.

The amount of coke produced can be reduced through the realization of appropriate active sites, but coke formation cannot be entirely prohibited considering the overall reaction. Therefore, enhancing the intrinsic resistivity of a catalyst to coke formation is essential for achieving a stable production of acrolein. In this regard, several attempts to control the textural properties of catalysts have been reported to improve coke resistivity. Tsukuda et al.^[20] studied the influence of mesopore size of the silica support on catalytic stability. They demonstrated that the silica with the largest pores had the best resistance, thereby emphasizing the importance of pore size in the stable production of acrolein. On the other hand, Hoang et al.^[21] examined suitable pore structures in terms of residence time of reactant or intermediate. They found that compounds containing alkyl and aromatic groups were primarily formed over a catalyst with a longer residence time, which resulted not only in a low selectivity for acrolein but also in a rapid deactivation of the catalyst by coke deposition. Although enhancing effects caused by large pores and suitable pore structure were deduced, the problem associated with deactivation was not solved.

Herein, we propose the use of an open-macropore-structured and Brønsted-acidic silica (Marigold-like silica functionalized with propanesulfonic acid groups, MS-FS) as a sustainable and selective catalyst for acrolein production. The appropriate Brønsted acid sites for the sequential dehydration of glycerol were obtained through functionalization with propanesulfonic acid groups. In the dehydration of glycerol, the open-macropore structure of the catalyst showed a clear enhancement in resistance to hard coke formation and to pore blocking by coke. Using DFT calculations, we found a relationship between the behavior of 3-HPA and the recyclability of Brønsted acid sites during sequential dehydration. The MS-FS catalyst permitted the deprotonated Brønsted acid sites to be easily regenerated, which led to the selective dehydration of 3-HPA into acrolein. Moreover, the formation of coke precursors originating from the degradation of 3-HPA was inhibited. For these reasons, the MS-FS catalyst showed outstanding selectivity for acrolein formation and was also quite stable (with yields approaching 73% after 50 h).

Results and Discussion

We designed and synthesized MS-FS (Scheme 1). The marigold-like structure accommodates the large open-pore space between the silica walls and can enhance the mass transport of both the reactant and product.^[22]



Scheme 1. Description of MS-FS catalyst on various scales.

The functionalization of the surface with propanesulfonic acid groups confers pure Brønsted-acid characteristics to the catalyst. The importance of Brønsted acid type has been emphasized in previous reports.^[7,14–17] In the case of acidity, a narrow distribution of acid strength should be advantageous for the selective formation of the product. In this regard, the propane-

Table 1. Effect of modification of the terminal carbon atom on ΔE_{DPE} of propanesulfonic acid and sulfuric acid: Cluster-based DFT calculations^[a]

| Model | Structure | Terminal group | $\Delta E_{\text{DPE}}^{\text{[b]}}$ [kJ mol ⁻¹] | Variation ^[c] [kJ mol ⁻¹] |
|--|-----------|------------------|--|--|
| CH ₃ (CH ₂) ₂ SO ₃ H | | – | 475.9 | – |
| CH ₃ (CH ₂) ₃ SO ₃ H | | CH ₃ | 475.8 | 0.1 |
| SiH ₃ (CH ₂) ₃ SO ₃ H | | SiH ₃ | 467.2 | 8.7 |
| AlH ₂ (CH ₂) ₃ SO ₃ H | | AlH ₂ | 472.7 | 3.2 |
| ZrH ₃ (CH ₂) ₃ SO ₃ H | | ZrH ₃ | 451.8 | 24.1 |
| H ₂ SO ₄ | | – | 427.2 | – |
| SiH ₃ SO ₄ H | | SiH ₃ | 422.4 | 4.8 |
| AlH ₂ SO ₄ H | | AlH ₂ | 369.7 | 42.5 |
| ZrH ₃ SO ₄ H | | ZrH ₃ | 323.3 | 103.9 |

[a] Computational details using cluster-based DFT calculation can be found in the Supporting Information. [b] With respect to following reaction: HA + NH₃ → A⁻ + NH₄⁺. [c] Difference of ΔE_{DPE} compared to CH₃(CH₂)₂SO₃H or H₂SO₄. Table 2

sulfonic acid moiety can ensure uniformity of acid strength because the propyl chain in the moiety separates the acid site from the surface of the catalyst. The variability of acid site strength induced from the surface structure^[23,24] can be diminished, resulting in acid sites with identical strengths. We confirmed this effect of propanesulfonic acid group by performing simple cluster-based DFT calculations (Table 1). The deprotonation energy (ΔE_{DPE} , related to the strength of acid sites) of propanesulfonic acid group was essentially unaltered ($\approx 24 \text{ kJ mol}^{-1}$) by the modification with a moiety attached to the terminal carbon atom. In contrast, a similar modification with sulfuric acid resulted in a significant change in ΔE_{DPE} ($\approx 104 \text{ kJ mol}^{-1}$).

Figure 1 shows electron microscope images of the MS-FS catalyst. It can be clearly seen that MS-FS is a nanosphere with a size ranging from 400–600 nm. The surface of MS-FS is covered by winding walls of silica, and deep canyons are formed between the walls (Figure 1a and c). In SEM images, the estimated distance between the silica walls ranges from 10 nm to over 100 nm. The thickness of each wall is estimated to be 13.1–17.5 nm based on Figure 1a, but it can be thinner because of the platinum coating required for SEM analysis. In Figure 1b, the wall thickness at the edge is about 3–5 nm. In the same image, pores formed between the silica walls are clearly observed. These pores appear to be formed from the inside to the outside of the nanospheres. In addition, very small white dots and fringes can be seen over the entire nanosphere. They are 2–5 nm-sized mesopores distributed in the silica walls and the inside of hierarchical structured pores, which was further confirmed by nitrogen physisorption analysis. Interestingly, although the propanesulfonic acid moieties were used to functionalize the catalyst, the overall catalyst structure was almost the same as that for a nonfunctionalized silica nanosphere [Marigold-like silica (MS), Figure S1].

Details concerning the pore structure and textural properties of the MS-FS catalyst were confirmed by nitrogen physisorption analysis. In the nitrogen isotherm plot (Figure 2a) of the MS and MS-FS catalysts, the broad hysteresis loop from 0.4 to 1.0 (P/P_0) indicates that meso- and macrosized pores are present in the catalysts. A significant increase in adsorbed nitrogen in the range of 0.7 to 1.0 clearly shows that there is a considerable amount of macropores in both catalysts. The most notable difference between the MS and MS-FS catalysts is the amount of adsorbed nitrogen near $P/P_0=0.4$. In the case of nonfunctionalized MS, a sharp increase in adsorbed nitrogen was observed, which implies the presence of large amounts of mesopores. In contrast, functionalized MS-FS does not show this sharp increase. The pore size distribution clearly shows this difference between the absence and presence of functional groups (Figure 2b). The amount of 2–5 nm-sized mesopores was definitely decreased as a result of functionalization. This can be attributed to the length of the propanesulfonic acid moiety (0.68–0.75 nm), which is sufficiently long to block small pores. In addition, this distinct difference in the amount of mesopores indicates that small mesopores

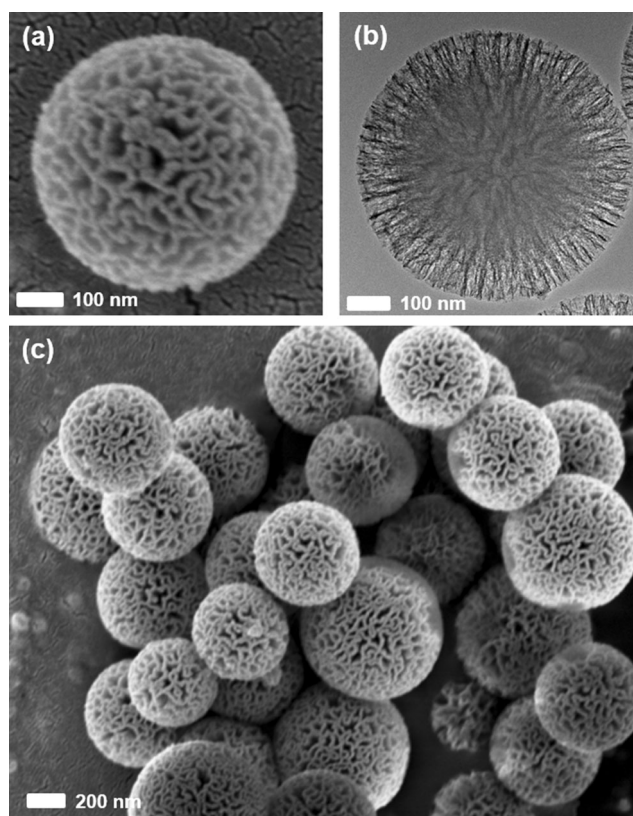


Figure 1. Electron microscope images of MS-FS catalyst: (a, c) SEM and (b) TEM.

are regularly distributed not only on the inside of hierarchically structured pores but also in the silica walls. This result is in good agreement with the observation of white dots and fringes in the TEM image (Figure 1b). The amount of macropores decreased because the thickening of the walls made the distance between the walls shorter. From these results, we confirmed that functionalization was successfully carried out and that hierarchically structured meso–macropores were well developed in the MS-FS catalyst.

Successful functionalization of MS-FS was also confirmed by elemental analysis (Table S1). In MS-FS, the weight percentage of sulfur was estimated to be 1.4%. In addition, the structure

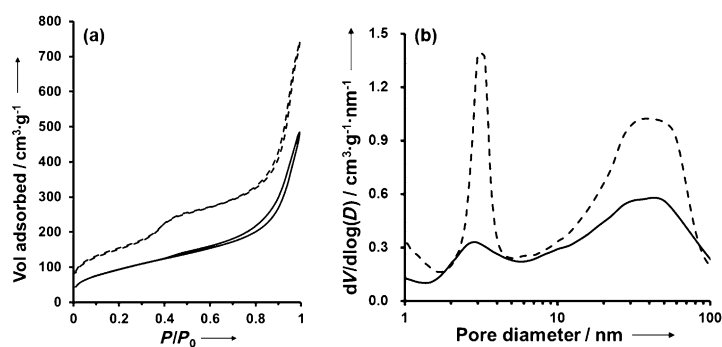


Figure 2. (a) N_2 adsorption-desorption isotherm and (b) pore size distribution curve of MS-FS (—) and MS (---).

of the functional groups was confirmed by FTIR analysis. In Figure S2, there is no peak at 2575 cm^{-1} , which indicates that the mercaptopropyl groups were fully oxidized to sulfonic acid groups.^[25,26] C–H vibrations at 2970 and 2873 cm^{-1} ^[27,28] and a hydroxyl band between 3200 and 3400 cm^{-1} ^[28] were identified and attributed to the presence of propyl groups and sulfonic acid groups, respectively.

The activity of the MS-FS catalyst was investigated for glycerol dehydration. Although the reaction was run for 50 h, the glycerol conversion was maintained at 100% and the selectivity for acrolein was high (72.8%; Figure 3). Considering previous studies, which attempted to solve the deactivation problem by co-feeding oxygen^[29] or adding a promoter,^[30–32] the selectivity for acrolein and the stability of MS-FS are outstanding. To further investigate the reason why MS-FS showed such a high stability, we carried out comparative studies with regard to i) hierarchically structured meso-macropores and ii) characteristics of Brønsted acid sites.

Extensive coke formation on the acid sites is a typical problem in glycerol dehydration.^[8,19] Coke deposition could lead to the blockage of pore entrances, resulting in rapid deactivation. Therefore, proper textural properties such as a large pore size and hierarchical pore structures are the major factors in terms of catalyst stability. For this reason, we selected zeolite HZSM-5 as a control group with microporous structures and compared the catalytic activities of both catalysts. Fresh HZSM-5 has a crystal structure, as evidenced by high-resolution (HR)-TEM (Figure S3) and XRD (Figure S4) analysis. Nitrogen adsorption-desorption isotherms showed no distinct hysteresis loop (Figure 4c), which indicates that the fresh HZSM-5 catalyst has a typical microporous structure unlike the MS-FS catalyst.

As shown in Table 2, HZSM-5 was initially active and selective for the production of acrolein (conversion 92.7% and selectivity 73.0%), similar to previous results.^[8] However, the catalyst was rapidly deactivated even though its selectivity was maintained. The conversion of glycerol after a 10 h reaction was only 21.9%. The major by-product, acetol, formed with the same selectivity (9.3%) using MS-FS, and other by-products formed at yields of nearly 0% for both catalysts.

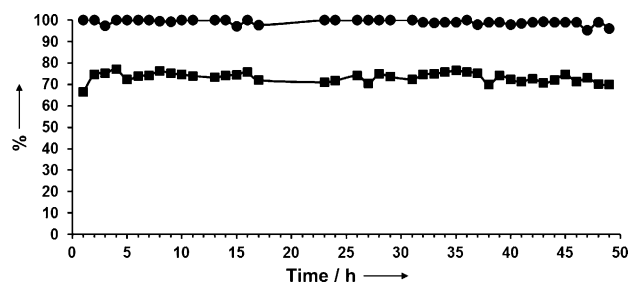


Figure 3. Glycerol conversion (●) and acrolein selectivity (■) of MS-FS.

The used catalysts were analyzed by using the nitrogen adsorption method, and a dramatic change in porosity was found. Figure 4a and b shows the pore size distribution of

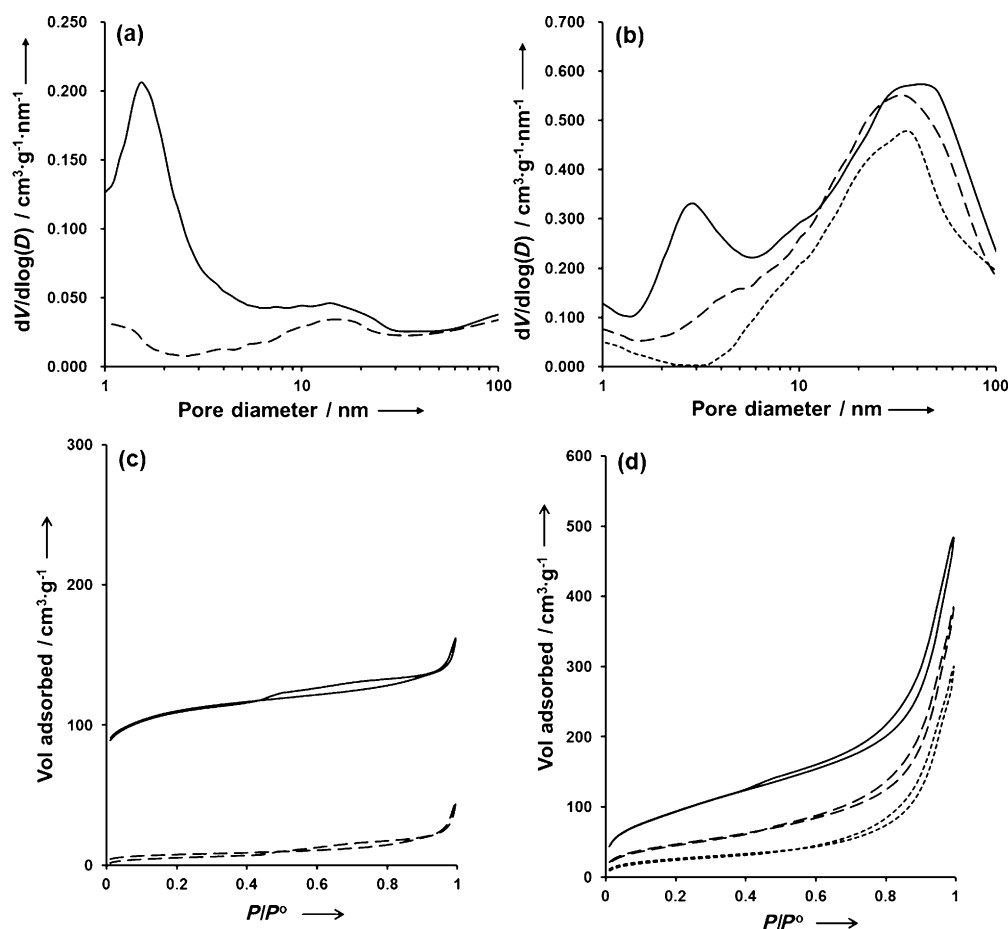


Figure 4. Pore size distribution of (a) HZSM-5 and (b) MS-FS catalysts for fresh samples (—) and those used for 10 (----) and 30 h (---). Nitrogen adsorption-desorption isotherms of (c) HZSM-5 and (d) MS-FS catalysts.

| Catalyst | Glycerol conversion [%] | | Selectivity [%] | | |
|----------|-------------------------|--------------|-----------------|--------|--------------|
| | TOS = 1–2 h | TOS = 9–10 h | acrolein | acetol | acetaldehyde |
| HZSM-5 | 92.7 | 21.9 | 73.0 | 9.3 | 0.0 |
| MS-FS | 100.0 | 100.0 | 73.4 | 9.3 | 0.0 |

HZSM-5 and MS-FS, respectively. In the case of HZSM-5, after 10 h reaction, the micro-sized pores were completely blocked due to coke deposition. In contrast, macropores of 20–100 nm in MS-FS were still present even after 30 h reaction. The difference between HZSM-5 and MS-FS is also presented in the isotherms of fresh and used samples (Figure 4c and d). The amount of adsorbed nitrogen for used HZSM-5 was significantly decreased in the range below 0.2 (P/P_0 ; region related to micropores), and the isotherm was down-shifted. On the other hand, most of the nitrogen adsorption ($P/P_0 > 0.6$) for the used MS-FS was still maintained. The results explain why the MS-FS catalyst showed a remarkable stability in spite of extensive coke formation. The hierarchically structured meso–macropores in MS-FS confer an advantage in that pore blocking is reduced, resulting that acid sites located inside the pores can remain functioning for a long reaction time.

In addition, the properties of the coke on the two catalysts were different from each other. Figure 5 shows the temperature-programmed oxidation (TPO) results for the used cata-

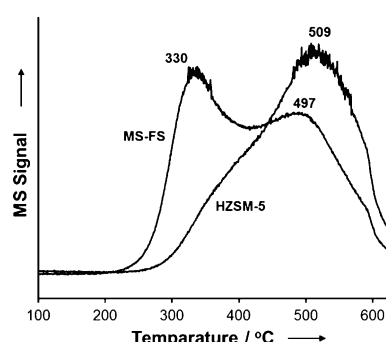


Figure 5. TPO-MS profiles of MS-FS and HZSM-5 after 10 h glycerol dehydration.

lysts. The oxidation of coke in MS-FS starts at 220 °C, which is a lower temperature compared with that for HZSM-5, 270 °C. In addition, the major oxidation peak appears at 330 °C in the MS-FS catalyst whereas that of HZSM-5 appears at 509 °C. This is because the coke in HZSM-5 is likely to be polymerized or condensed due to the microporous structure of the catalyst. Also, by comparing the integrated area of TPO profiles in both catalysts, it can be seen that the amount of coke produced is similar. As frequently pointed out, the stability of MS-FS is superior to HZSM-5 although a similar amount of coke was deposited during the reaction. These results can be explained by a study reported by Hoang et al.^[21] In the meso–macropores of MS-FS, the residence time of intermediates or coke precursors can be reduced, which results in a decrease in the probability of coke polymerization.

A comparison of the Brønsted acid sites was carried out using sulfated zirconia supported on the marigold-like silica (SZ/MS) and MS-FS catalysts. The morphology of the SZ/MS catalyst was confirmed to be identical with that of MS-FS (Figure 6a–d); the use of the same morphology can diminish the effect of pore structure. As shown in the 2D energy dispersive X-ray spectroscopy (EDS) mapping images of SZ/MS (Fig-

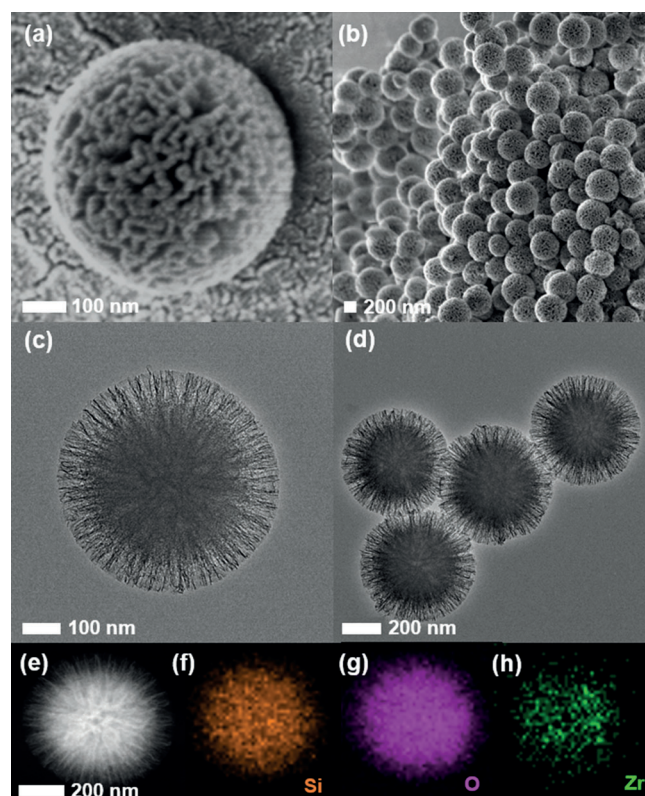


Figure 6. (a, b) SEM, (c, d) HR-TEM, (e) high-angle annular dark-field scanning transmission electron microscope (HAADF-STEM), and (f–h) EDS mapping images of the SZ/MS catalyst.

ure 6e–h), sulfated zirconia was highly dispersed on the MS support. Only a broad amorphous silica peak corresponding to SZ/MS is observed in Figure S4, which is also consistent with the sulfated zirconia being highly dispersed in the SZ/MS catalyst. The loaded amount of sulfur was estimated by elemental analysis (Table S1). The weight percentage of sulfur in the SZ/MS is same as that in the MS-FS catalyst. This indicates that the amount of functional groups is identical in both fresh MS-FS and SZ/MS catalysts.

The acid sites of the sulfated zirconia exhibit Brønsted-acidic characteristics that are structurally similar to the sulfonic acid moiety of MS-FS.^[33] The major differences in acid sites between SZ/MS and MS-FS are acid strength and uniformity of acid site distribution. Temperature-programmed desorption of NH_3 (NH_3 -TPD) results for MS-FS and SZ/MS are presented in Figure 7. NH_3 desorption in the case of MS-FS started at 100 °C and ended at around 300 °C. In the case of SZ/MS, the desorbed NH_3 was detected in the broad temperature range from 120–480 °C. The higher temperature of NH_3 desorption in the case of SZ/MS suggests that the SZ/MS catalyst exhibit a slightly stronger acidity than the MS-FS catalyst. Moreover, MS-FS showed a narrower NH_3 desorption peak than SZ/MS, which indicates that acid sites in MS-FS are uniformly distributed. This result is consistent with cluster-based DFT calculation results. Considering the uniform distribution of the acid sites, the selectivity for acrolein of MS-FS was expected to be superior to that of SZ/MS.

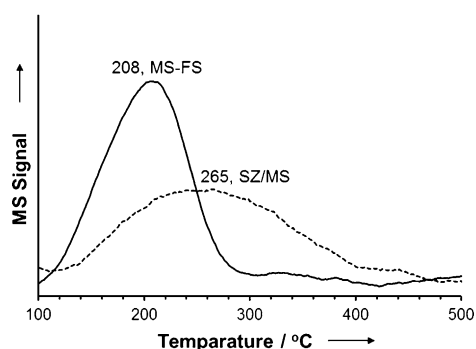


Figure 7. NH_3 -TPD-MS profiles of MS-FS and SZ/MS.

Experimental results show that the SZ/MS catalyst has a low glycerol conversion and selectivity for acrolein, which is a completely different to the result for the MS-FS catalyst (Table 3). The deactivation behavior in SZ/MS was also distinct from that of MS-FS. Even though both catalysts have almost identical

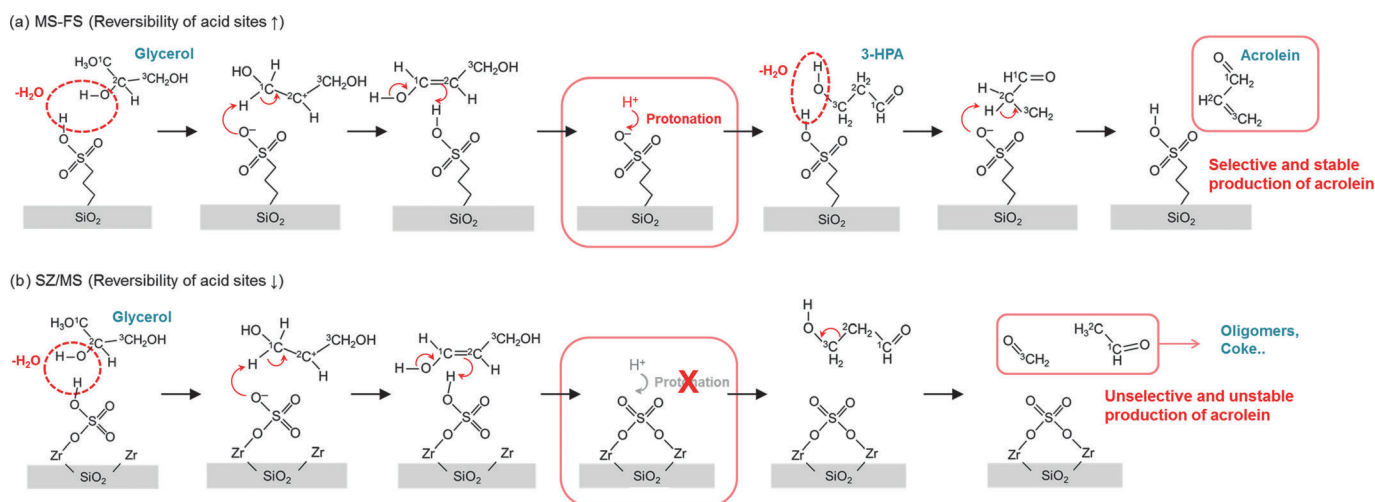
| Catalyst | Glycerol conversion [%] | | Selectivity [%] | | |
|----------|-------------------------|--------------|-----------------|--------|--------------|
| | TOS = 1–2 h | TOS = 9–10 h | acrolein | acetol | acetaldehyde |
| SZ/MS | 76.8 | 56.8 | 18.3 | 10.7 | 8.6 |
| MS-FS | 100.0 | 100.0 | 73.4 | 9.3 | 0.0 |

textural properties, glycerol conversion using SZ/MS decreased with increasing time on stream (TOS). After the reactions, we analyzed the amount of sulfur in both used catalysts because sulfonic acid groups or sulfuric acid groups can be detached from the silica support. The weight percentage of sulfur remained unchanged in both catalysts (Table S1). This indicates that the main reason for the deactivation of SZ/MS is not the leaching of sulfur from the catalyst or pore blocking.

The low selectivity for acrolein is explained by the fact that SZ/MS has a stronger acid strength than MS-FS. Too strong Brønsted acid sites could result in a significant formation of by-products because many side reactions are also catalyzed by Brønsted acid sites during glycerol dehydration.^[13] However, the formation of a considerable amount of acetaldehyde (8.6% in SZ/MS) cannot be solely explained by the difference in acid strength. It was reported that the formation of acetaldehyde stems from the homogeneous decomposition of 3-HPA.^[10,15,34] Therefore, the formed 3-HPA was preferentially desorbed from the acid sites of the SZ/MS catalyst and then homogeneous decomposition to acetaldehyde occurred. To explain such a difference, we anticipated that the ‘reversibility’ of the Brønsted acid site was the reason for the difference between the MS-FS and SZ/MS catalysts. Herein, the term reversibility is similar to the ability of recovering protons from reaction intermediates.

Scheme 2 shows a proposed reaction mechanism accounting for the reversibility of each catalyst. In both catalysts, glycerol is converted into 3-HPA through protonation and dehydration. After this, in the case of the easily reversible MS-FS catalyst, a proton is readily transferred to an acid site to regenerate the Brønsted acidity. Over regenerated sites, 3-HPA is readily adsorbed on an acid site by hydrogen bonding and selectively dehydrated to acrolein. In contrast, the reversibility of SZ/MS is somewhat lower than that of MS-FS, and the recovery of a proton for SZ/MS is more difficult than for MS-FS. When the deprotonated sites are readily regenerated in SZ/MS, the reaction of 3-HPA would follow the same route as that on the MS-FS catalyst. On the other hand, when deprotonated sites are not regenerated, 3-HPA can be desorbed from the active site due to the absence of interactions and would decompose into formaldehyde and acetaldehyde. These compounds can participate in side reactions to form coke.^[10,12,15] Therefore, we expect that this difference is the reason why the SZ/MS catalyst exhibits different catalytic activities compared to the MS-FS catalyst.

To verify the proposed scheme, we compared the recyclability of acidic protons for each catalyst using DFT calculations. In



Scheme 2. Proposed mechanism concerning recyclability of a Brønsted acid site in (a) MS-FS and (a) SZ/MS catalysts

the elementary steps of a typical dehydration,^[14] the reaction is initiated by the migration of a proton from a Brønsted acid site to the reactant. Then, the protonated reactant undergoes dehydration and a charged intermediate is formed. Finally, the proton is pulled out from the charged intermediate with the Brønsted acidity being recovered. As already noted, we anticipate that the last step is probably important in the sequential dehydration of glycerol.

In the calculation, a water molecule was used as a probe to investigate the recyclability of the MS-FS and SZ/MS catalysts. Figure 8 shows the optimized structures for the overall dehy-

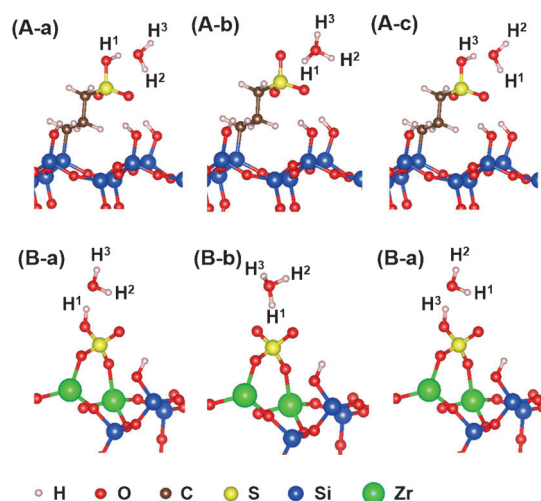


Figure 8. (a, c) Adsorption geometries and (b) transition state for water-assisted proton transfer reaction on (A) MS-FS and (B) SZ/MS catalysts.

dration process, which consists of the adsorption of water, proton transfer from a Brønsted acid site to water, and the recovery of a proton from a hydronium ion. To describe proton transfer and recovery, we simulated a water-assisted proton exchange. The adsorption energies of water on the MS-FS and SZ/MS surfaces were -39.8 and -49.6 kJ mol^{-1} , respectively. The activation energy required for the transfer of a proton from MS-FS was 111.4 kJ mol^{-1} , which was higher than that for SZ/MS (79.2 kJ mol^{-1} , Figure 9). This result is consistent with experimental observations (NH_3 -TPD-MS, Figure 7) because the

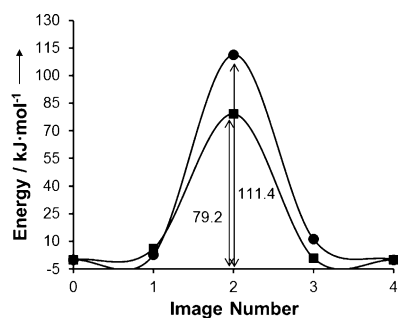


Figure 9. DFT calculations of the minimum energy path for water-assisted proton exchange over MS-FS (●) and SZ/MS (■) surfaces.

lower protonation energy corresponds to a catalyst with a stronger acidity. At the same time, however, the recovery of a proton from a hydronium ion over the MS-FS catalyst is more thermodynamically favored than the analogous process for SZ/MS due to the higher stabilization energy of proton extraction (-111.4 vs. -79.2 kJ mol^{-1}). Therefore, the recyclability of SZ/MS was inferior to that of MS-FS, which resulted in the generation of deprotonated acid sites. Over the deprotonated acid sites, the adsorption of 3-HPA was not favorable as the calculated energy was only -1.9 kJ mol^{-1} , which was negligible compared to -56.2 kJ mol^{-1} for the initial acid site (Figure S5). In this situation, 3-HPA can be readily desorbed from the site and decomposition to acetaldehyde and formaldehyde would be expected to follow. Based on these computational calculations, we confirmed that the proposed reaction mechanism in MS-FS and SZ/MS catalysts is reasonable. In addition, it cannot be emphasized enough that not only appropriate acidity but also the recyclability of acid sites is a crucial factor for the selective and stable production of acrolein in the sequential dehydration of glycerol.

Conclusions

We designed and successfully synthesized a hierarchical-pore-structured and propanesulfonic-acid-functionalized silica catalyst (MS-FS) to stably produce acrolein from glycerol. As expected, the MS-FS catalyst showed an outstanding selectivity ($\approx 73\%$) and stability (50 h) during the sequential dehydration of glycerol to acrolein. Compared to a microporous HZSM-5 zeolite, the hierarchically structured meso-macropores in MS-FS were strongly resistant to the blocking of pore entrances by coke deposition. Moreover, the formed coke was confirmed to be more easily oxidized than the highly condensed coke formed in the case of HZSM-5. As a consequence, acrolein was stably produced using the MS-FS catalyst, even after a considerable amount of coke had been deposited.

In addition, we found that the recyclability of deprotonated Brønsted acid sites is a significant factor in the sequential dehydration of glycerol. If the recyclability of a catalyst is sufficient, the regeneration of deprotonated Brønsted acid site easily takes place. In this case, 3-HPA formed from the first dehydration of glycerol is favorably adsorbed onto the regenerated Brønsted acid site followed by dehydration into acrolein in the subsequent step. However, in the case of a catalyst with a low recyclability, the regeneration of the deprotonated acid sites is retarded and the probability of 3-HPA being desorbed from the active site increases, resulting in a high likelihood of decomposition into acetaldehyde and formaldehyde. DFT calculations revealed that the MS-FS catalyst had an improved regeneration ability of deprotonated Brønsted acid sites compared to that of sulfated zirconia supported on silica (SZ/MS). Therefore, the sequential dehydration is easily achieved in the case of the MS-FS catalyst with a high selectivity for acrolein. Furthermore, catalyst stability is also enhanced because the formation of coke precursors generated from the degradation of 3-HPA is inhibited at the regenerated acid sites.

Experimental Section

Preparation of catalysts

MS-FS was synthesized by a water-in-oil microemulsion process using a hydrothermal reactor. A synthetic method for marigold-like silica (MS) was published by Park et al.^[22] Urea (0.6 g) and cetylpyridinium bromide (1.0 g) were dissolved in water (30 mL). Tetraethyl orthosilicate (2.5 g), pentanol (1.5 mL), and cyclohexane (30 mL) were mixed. The two solutions were mixed for 30 min, and the mixture was prehydrolyzed at 120 °C for 2.5 h in an autoclave while stirring. After the reaction, the sample was cooled to room temperature and 3-mercaptopropyl trimethoxy silane (0.62 g) was slowly added while stirring. The sample was prepared in the same way as for prehydrolyzation, with the only difference being a 4 h reaction time. The product was centrifuged three times using a mixture of deionized water (15 mL) and acetone (15 mL). After that, the resulting material was dried at room temperature and grinded to a fine powder. To remove the surfactant, ethanol extraction was conducted because the functional groups can be oxidized through heat treatment or calcination. The sample (1 g) was suspended in ethanol (250 mL). After stirring at 75 °C for 24 h, a precipitate was obtained by centrifugation and dried at room temperature. Then, the sample (1 g) was oxidized using hydrogen peroxide (80 g; 34.5 wt%) at 60 °C for 24 h followed by washing with deionized water and ethanol. Finally, the product was dried at 70 °C for 12 h. Zirconia supported on silica (7 wt%) was synthesized using an incipient wetness impregnation method. Zirconium oxychloride was dissolved in deionized water, and the marigold-like silica was impregnated with the solution. The sample was then dried at 80 °C overnight and calcined at 300 °C for 2 h. The calcined sample (0.5 g) was treated with sulfuric acid (10 mL; 0.5 M, 95%) at room temperature for 30 min and calcined again at 650 °C for 3 h.

Catalyst characterization

To record the morphology of the samples, we carried out electron microscopy. HR-TEM and SEM images were obtained using a JEOL JEM-3010 and SUPRA 55VP microscope, respectively. An analytical high-angle annular dark-field scanning transmission electron microscope (HAADF-STEM, Tenai F20-FEI, 200 kV) equipped with EDS (Tecnai 136-5-EDAX) was used for elemental mapping of the sample. Nitrogen adsorption-desorption isotherms were recorded on a Micromeritics ASAP-2010, and the pore size distribution was determined from the branches of the isotherm using the Barrett-Joyner-Halenda method. Elemental analysis (CHNSO932, LECO) was conducted to determine the amount of sulfur in samples before and after the reaction. XRD patterns were obtained at angles ranging from 10–80° using a Rigaku D-MAX2500-PC powder X-ray diffractometer with $\text{CuK}\alpha$ radiation (1.5406 Å). The chemical structure of the catalyst was confirmed using a FTIR spectrophotometer (Nicolet 6700, Thermo Scientific). TPO and NH_3 -TPD results were obtained using a Micromeritics Autochem II chemisorption analyzer with an on-line mass spectrometer (QGA, Hiden Analytical). In the case of TPO analysis, the sample was loaded onto the reactor and heated up to 100 °C under a helium flow to vaporize the physically adsorbed molecules. After waiting for 1 h, the temperature was cooled to 50 °C. The data was collected while the temperature was increased to 600 °C at a rate of 5 °C min^{-1} under a flow of 10% O_2/He . In the case of NH_3 -TPD analysis, the sample was pretreated with 10.2% NH_3/He gas at 50 °C. The temperature was increased to 100 °C under a He flow to eliminate physisorbed NH_3 . After removing physisorbed NH_3 , the temperature was cooled

to 50 °C and increased again to 600 °C (10 °C min^{-1}) under a flow of helium. The data was collected simultaneously.

Catalytic activity test

The catalytic activity test was conducted at 250 °C in a fixed-bed quartz reactor. Before the reaction, the catalyst was pretreated at 250 °C for 30 min under a flow of N_2 (30 mL min^{-1}). For the long-term stability test of MS-FS, the catalyst (0.45 g) was loaded and a glycerol solution (1.2 M) was fed into the reactor using a syringe pump at a rate of 1.5 mL h^{-1} under a flow of nitrogen (30 mL min^{-1}). For the comparison test, the catalyst (0.3 g) was loaded and a glycerol solution (1.2 M) was fed into the reactor using a syringe pump at a rate of 2.0 mL h^{-1} to exactly observe the difference in catalytic activities. When the glycerol solution was injected, the temperature of the inlet line was heated to 270 °C to vaporize the reactant. After the gas-phase glycerol reacted, the products were condensed in a cold trap and analyzed using a gas chromatograph (Younlin ACME 6100) equipped with a flame ionization detector (FID) and an HP-Innowax capillary column.

Computational details

Plane-wave DFT calculations were performed using the Vienna Ab-initio Simulation Package (VASP) code^[35] implementing the generalized gradient approximation (GGA) of Perdew-Burke-Ernzerhof (PBE) exchange-correlation functional.^[36] As an all-electron description, the projector augmented wave method (PAW) was used.^[37] The energy cut-off for the plane-wave basis set expansion was set to 400 eV and the Brillouin zone was sampled using a $3 \times 3 \times 1$ Monkhorst-Pack k -point mesh. All structures were optimized until forces on all atoms were converged to $< 0.03 \text{ eV \AA}^{-1}$. The electronic optimization steps were converged to $< 2 \times 10^{-4} \text{ eV}$.

The model surfaces of propanesulfonic acid functionalized silica (MS-FS) and SZ/MS were constructed based on the model of Rozanska et al.^[38] The (111) surface of β -cristobalite was used as the model to represent amorphous silica surface.^[39–41] Physical properties, such as refractive index and bulk density, of β -cristobalite fairly resemble those of amorphous silica.^[42,43] The most preferred structure was found through careful examination of possible structures, for example, location of propanesulfonic acid group and zirconium ion on the silica surface, and rotating angle between the surface and propanesulfonic acid group. In our calculations, all atomic positions were fully relaxed to move, and a sufficient distance between the two adjacent slabs was provided to avoid periodic interactions.

The climbing image-nudged elastic band (CI-NEB) method^[44,45] was used to determine transition states and energy barriers for the proton-exchange ability of the catalysts. A $1 \times 1 \times 1$ Monkhorst-Pack k -point mesh and a cut-off energy of 400 eV were used for these calculations. Initial reaction trajectories consisted of three images obtained through linear interpolation. To determine minimum energy paths, these images were optimized until the forces between the images fell to $< 0.06 \text{ eV \AA}^{-1}$.

Acknowledgements

This work was financially supported by a grant from the Industrial Source Technology Development Programs (2013-10033352) of the Ministry of Trade, Industry and Energy (MOTIE) of Korea. This research was also supported by the Supercomputing Center/

Korea Institute of Science and Technology Information with supercomputing resources including technical support (KSC-2013-C1-025). This work was also supported by the National Research Foundation of Korea (NRF) grant funded by the Korea government (MEST) (No.2013R1A2A2A01067164).

Keywords: brønsted acid · coke resistivity · dehydration · glycerol · hierarchical pore structure

- [1] R. Slade, R. Gross, A. Bauen, *Energy Environ. Sci.* **2011**, *4*, 2645–2657.
- [2] M. I. Hoffert, K. Caldeira, G. Benford, D. R. Criswell, C. Green, H. Herzog, A. K. Jain, H. S. Keshgi, K. S. Lackner, J. S. Lewis, H. D. Lightfoot, W. Manheimer, J. C. Mankins, M. E. Mauel, L. J. Perkins, M. E. Schlesinger, T. Volk, T. M. L. Wigley, *Science* **2002**, *298*, 981–987.
- [3] C. H. Zhou, X. Xia, C. X. Lin, D. S. Tong, J. Beltramini, *Chem. Soc. Rev.* **2011**, *40*, 5588–5617.
- [4] A. J. Ragauskas, Ch. K. Williams, B. H. Davison, G. Britovsek, J. Cairney, C. A. Eckert, W. J. Frederick, J. P. Hallett, D. J. Leak, C. L. Liotta, J. R. Mielenz, R. Murphy, R. Templer, T. Tschaplinski, *Science* **2006**, *311*, 484–489.
- [5] G. W. Huber, A. Corma, *Angew. Chem. Int. Ed.* **2007**, *46*, 7184–7201; *Angew. Chem.* **2007**, *119*, 7320–7338.
- [6] A. Corma, S. Iborra, A. Velty, *Chem. Rev.* **2007**, *107*, 2411–2502.
- [7] A. Alhanash, E. F. Kozhevnikova, I. V. Kozhevnikov, *Appl. Catal. A* **2010**, *378*, 11–18.
- [8] B. Katryniok, S. Paul, V. Bellière-Baca, P. Rey, F. Dumeignil, *Green Chem.* **2010**, *12*, 2079–2098.
- [9] B. Katryniok, S. Paul, M. Capron, F. Dumeignil, *ChemSusChem* **2009**, *2*, 719–730.
- [10] A. Corma, G. W. Huber, L. Sauvanaud, P. O'Connor, *J. Catal.* **2008**, *257*, 163–171.
- [11] L. Liu, X. P. Ye, J. J. Bozell, *ChemSusChem* **2012**, *5*, 1162–1180.
- [12] W. Suprun, M. Lutecki, T. Haber, H. Papp, *J. Mol. Catal. A* **2009**, *309*, 71–78.
- [13] X. Lin, Y. Lv, Y. Qu, G. Zhang, Y. Xi, D. L. Phillips, C. Liu, *Phys. Chem. Chem. Phys.* **2013**, *15*, 20120–20133.
- [14] K. Kongpatpanich, T. Nanok, B. Boekfa, M. Probst, J. Limtrakul, *Phys. Chem. Chem. Phys.* **2011**, *13*, 6462–6470.
- [15] S. H. Chai, H. P. Wang, Y. Liang, B. Q. Xu, *Green Chem.* **2007**, *9*, 1130–1136.
- [16] C. J. Jia, Y. Liu, W. Schmidt, A. H. Lu, F. Schüth, *J. Catal.* **2010**, *269*, 71–79.
- [17] Y. Choi, D. S. Park, H. J. Yun, J. Baek, D. Yun, J. Yi, *ChemSusChem* **2012**, *5*, 2460–2468.
- [18] Y. T. Kim, S. J. You, K. D. Jung, E. D. Park, *Bull. Korean Chem. Soc.* **2012**, *33*, 2369–2377.
- [19] B. Katryniok, S. Paul, M. Capron, V. Bellière-Baca, P. Rey, F. Dumeignil, *ChemSusChem* **2012**, *5*, 1298–1306.
- [20] E. Tsukuda, S. Sato, R. Takahashi, T. Sodesawa, *Catal. Commun.* **2007**, *8*, 1349–1353.
- [21] T. Q. Hoang, X. Zhu, T. Danuthai, L. L. Lobban, D. E. Resasco, R. G. Mallinson, *Energy Fuels* **2010**, *24*, 3804–3809.
- [22] D. S. Park, D. Yun, Y. Choi, T. Y. Kim, S. Oh, J. H. Cho, J. Yi, *Chem. Eng. J.* **2013**, *228*, 889–895.
- [23] M. A. Ecomier, K. Wilson, A. F. Lee, *J. Catal.* **2003**, *215*, 57–65.
- [24] M. Brändle, J. Sauer, *J. Am. Chem. Soc.* **1998**, *120*, 1556–1570.
- [25] W. M. Van Rhijn, D. E. D. Vos, B. F. Sels, W. D. Bossaert, P. A. Jacobs, *Chem. Commun.* **1998**, 317–318.
- [26] E. Cano-Serrano, J. M. Campos-Martin, J. L. G. Fierro, *Chem. Commun.* **2003**, 246–247.
- [27] D. Margolese, J. A. Melero, S. C. Christiansen, B. F. Chmelka, G. D. Stucky, *Chem. Mater.* **2000**, *12*, 2448–2459.
- [28] Y. K. Oh, L. Y. Hong, Y. Asthana, D. P. Kim, *J. Ind. Eng. Chem.* **2006**, *12*, 911–917.
- [29] F. Wang, J. L. Dubois, W. Ueda, *J. Catal.* **2009**, *268*, 260–267.
- [30] B. Katryniok, S. Paul, M. Capron, C. Lancelot, V. Bellière-Baca, P. Rey, F. Dumeignil, *Green Chem.* **2010**, *12*, 1922–1925.
- [31] P. Lauriol-Garbey, S. Loridant, V. Bellière-Baca, P. Rey, J. M. M. Millet, *Catal. Commun.* **2011**, *16*, 170–174.
- [32] D. S. Park, B. K. Kwak, N. D. Kim, J. R. Park, J. H. Cho, S. Oh, J. Yi, *ChemCatChem* **2012**, *4*, 836–843.
- [33] F. Cavani, S. Guidetti, C. Trevisanut, E. Ghedini, M. Signoretto, *Appl. Catal. A* **2011**, *409–410*, 267–278.
- [34] M. R. Nimlos, S. J. Blanksby, X. Qian, M. E. Himmel, D. K. Johnson, *J. Phys. Chem. A* **2006**, *110*, 6145–6156.
- [35] G. Kresse, J. Furthmüller, *Phys. Rev. B* **1996**, *54*, 11169–11186.
- [36] J. P. Perdew, K. Burke, M. Ernzerhof, *Phys. Rev. Lett.* **1996**, *77*, 3865–3868.
- [37] P. E. Blöchl, *Phys. Rev. B* **1994**, *50*, 17953–17979.
- [38] X. Rozanska, F. Delbecq, P. Sautet, *Phys. Chem. Chem. Phys.* **2010**, *12*, 14930–14940.
- [39] F. Vigné-Maeder, P. Sautet, *J. Phys. Chem. B* **1997**, *101*, 8197–8203.
- [40] J. Handzlik, J. Ogonowski, *J. Phys. Chem. C* **2012**, *116*, 5571–5584.
- [41] J. Handzlik, *J. Phys. Chem. C* **2007**, *111*, 9337–9348.
- [42] D. W. Sindorf, G. E. Maciel, *J. Am. Chem. Soc.* **1983**, *105*, 1487–1493.
- [43] I. S. Chuang, G. E. Maciel, *J. Phys. Chem. B* **1997**, *101*, 3052–3064.
- [44] G. Henkelman, H. Jonsson, *J. Chem. Phys.* **2000**, *113*, 9978–9985.
- [45] G. Henkelman, B. P. Uberuaga, H. Jonsson, *J. Chem. Phys.* **2000**, *113*, 9901–9904.

Received: February 13, 2014

Published online on July 8, 2014